On the Onset of Plasticity: Determination of Strength and Ductility

Alan F. Jankowski1

Correspondence: Alan Jankowski, Sandia National Laboratory, PO Box 969, Livermore CA., 94551-0969, USA. Tel: 1-925-294-2742. E-mail: afjanko@sandia.gov

Received: May 3, 2024 Accepted: June 5, 2024 Online Published: June 10, 2024

Abstract

The analysis of the work hardening variation with stress reveals insight to operative stress-strain mechanisms in material systems. The onset of plasticity can be assessed and related to ensuing plastic deformation up to the structural instability using one constitutive relationship that incorporates both behaviors of rapid work hardening (Stage 3) and the asymptotic leveling of stress (Stage 4). Results are presented for the mechanical behavior analysis of Ti-6Al-4V wherein the work hardening variation of Stages 3 and 4 are found to: be dependent through a constitutive relationship; be useful in a Hall-Petch formulation of yield strength; and provide the basis for a two point-slope fit method to model the experimental work hardening and stress-strain behavior.

Keywords: plasticity, work hardening, stress-strain, yield strength

1. Introduction

The use of the work hardening variation $\Theta(\sigma)$ with stress is shown (Jankowski, 2023a; Jankowski 2023b) to be integrally related to three fundamental stress-strain $\sigma(\epsilon)$ laws. The work hardening assessment establishes the relationships between: a linear $\Theta(\sigma)$ behavior and the Voce (1948) expression; a negative power law $\Theta(\sigma)$ behavior and the Hollomon (1945) expression; and a negative exponential $\Theta(\sigma)$ behavior with a new (Jankowski, 2023a) logarithmic $\sigma(\epsilon)$ behavior. The plastic strain beyond the proportional limit to the instability, as defined by the Considère (1885) criteria, can be well described from these expressions. These three relationships are illustrated in Figure 1. Herein, consideration is given to the rapid increase in $\Theta(\sigma)$ that occurs after the proportional limit in Stage 3, and the leveling in $\Theta(\sigma)$ which occurs in Stage 4, prior to Stage 5 that occurs beyond the instability of localized necking to fracture. The fluctuations in stress that can be associated with dislocation glide in Stages 1 and 2 are not addressed as these stages are not usually observed in polycrystalline materials.

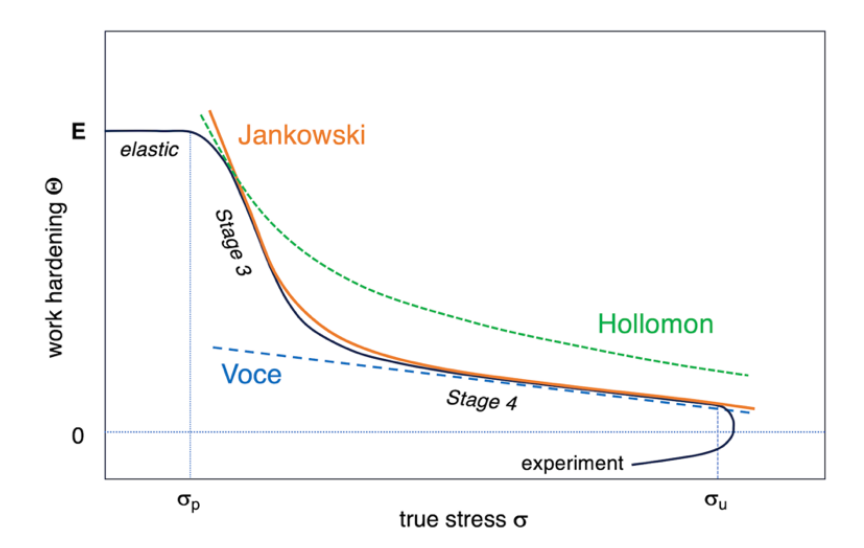


Figure 1. A schematic of three models that illustrate the work hardening variation $\Theta(\sigma)$ for the dominant stages of plasticity from beyond the proportional limit up to the instability.

¹ Sandia National Laboratory, Livermore, CA, USA

In a direct formulation of work hardening, the Voce expression leads to a Kocks-Mecking relationship (Kocks & Mecking, 2003; Jankowski 2023c) wherein a linear $\Theta(\sigma)$ decay occurs in Stage 4 beyond the yield strength up to the instability. In comparison, the negative exponential expression (Jankowski, 2023d) for $\Theta(\sigma)$ produces an asymptotic behavior for $\sigma(\varepsilon)$ and the $\Theta(\sigma)$ in Stage 4. Also, rather than using an additional linear $\Theta(\sigma)$ relationship based on the Voce relationship to define the Stage 3 onset of plasticity from the proportional limit up to the offset strain that defines a yield strength, the negative-exponential relationship provides a single $\Theta(\sigma)$ expression that spans both stages of plasticity. The use of the Kocks-Mecking coefficient (k) to describe $\Theta(\sigma)$ behavior is limited to the linear response in just Stage 4. The softening coefficient (c_b) is used (Morris, Jr., 2007; Jankowski et al., 2019) to describe an integrated linear $\Theta(\sigma)$ behavior for Stages 3-4, although the slopes are widely different for each stage. Despite these limitations, the approach of using a softening coefficient (cb;) for the stages of work hardening provides a straightforward means to define the useful plasticity of a material as, e.g., it may change due to a consequence of synthesis method as well as post-processing conditions. This approach of determining chivalues has proven to be a successful path to differentiate the effect of process parameters in the evaluation of additively manufactured (AM) alloys such as 304L (Jankowski & Yee, 2023a), 316L (Jankowski et al., 2020), Ti-6Al-4V (Jankowski, 2021), and Al 6061 (Jankowski & Yee, 2023b). The analysis of the formalisms further developed (Jankowski, 2023a) to detail the inter-relationships between $\sigma(\varepsilon)$ and $\Theta(\sigma)$ reveal insight to the onset of plastic deformation, as typically referred to as Stage 3 of the Kocks-Mecking $\Theta(\sigma)$ behavior. Additional analysis of Stage 3 in a $\Theta(\sigma)$ plot is pursued with respect to the determination of the: yield strength σ_v ; activation volume v^* of dislocations upon the onset of plasticity; and extent of plasticity in Stage 4 - as functionally interrelated by coefficients c_{b_3} and c_{b_4} that asymptotically approximate the curvilinear regions of these sequential work hardening stages.

2. Method

2.1 The Onset of Plasticity

For the work hardening approaches described, the onset of plasticity can be described by a linear slope (c_{b_3}) to the curve that describes the rapid decent in the curvilinear response of $\Theta(\sigma)$ in Stage 3. A derivation shows (Jankowski, 2023a) that the product of the activation volume (v^*) with the strain-rate sensitivity of strength exponent (m) as defined through the Dorn relationship where strength is proportional to strain rate raised to the power m, is directly proportional to the softening coefficient c_{b_3} as expressed in eqn. (1).

$$\mathbf{m} \cdot \mathbf{v}^* = \mathbf{c}_{\mathbf{v}^*} \cdot \mathbf{c}_{\mathbf{b}_2} \tag{1}$$

The coefficient c_{v^*} in eqn. (1) is numerically determined using eqn. (2) where: the elastic modulus (E) is the value of $\Theta(\sigma)$ in Stage 2; Θ_{o_3} is the $\Theta(0)$ intercept for Stage 3 at zero stress (σ); T is the temperature absolute; and k_B is the Boltzmann constant.

$$c_{v^*} = k_B \cdot T / (\Theta_{o_3} - E) \tag{2}$$

General observations (Dao et al., 2007; Wei et al., 2004; Gu et al., 2007; Nyakiti & Jankowski, 2010; Jankowski & Nyakiti, 2010; Humphrey & Jankowski, 2011) of the mechanical properties of materials reveals relationships between the plasticity, strength, and activation volume that are summarized in the schematic plot of Figure 2 for the variation in the strain-rate sensitivity of strength exponent (m) as a function of grain size hg from the nanothrough micro- to macro- scale.

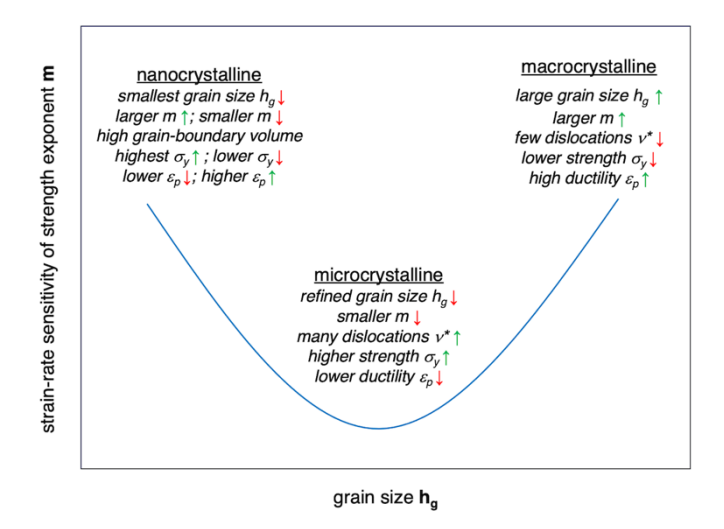


Figure 2. The trends observed within the variation of strain-rate sensitivity exponent (m) with grain size (hg) are summarized from the nano- through micro- to macro- scale affecting the strain-rate sensitivity of dislocation based-strengthening.

Beyond the complexities of the transitioning into the nanocrystalline range of materials, the mechanical properties of interest for the advanced manufacturing of alloys takes form in the micro-to-macro crystalline range. The greater ductility ε_p and lower strength σ_y of materials that occurs when grain size h_g increases from the micro-to-macro crystalline is associated with a greater strain-rate sensitivity exponent m and a smaller activation volume v^* of dislocations upon yielding. The $m \cdot v^*$ product of eqn. (1) is found to be proportional to the slope (c_{b3}) of work hardening $\Theta(\sigma)$ in Stage 3. The value of the Stage 3 intercept (Θ_{o3}) will algebraically decrease with a decreasing Stage 3 slope (c_{b_3}) as stress increases. In general, this relationship indicates that lower strengths can be associated with greater Θ_{o3} and c_{b_3} values. An expectation (Jankowski, 2023a) consistent with this behavior of strength σ decreasing as c_{b_3} increases, is that the slope c_{b_4} of the continued curvilinear $\Theta(\sigma)$ behavior into Stage 4 will increase as c_{b_3} decreases and the yield strength σ increases. Here, strength can be denoted (Jankowski, 2023a) by the proportional limit σ_p , or an offset yield strength σ_d that marks the transition between Stage 3 and 4 work hardening. These predicted trends in work hardening, as shown in Figure 3, can now be assessed for a set of mechanical property data (Jankowski & Yee, 2023a; Jankowski, et al., 2020; Jankowski, 2021; Jankowski & Yee, 2023b) of additively manufactured Ti-6Al-4V.

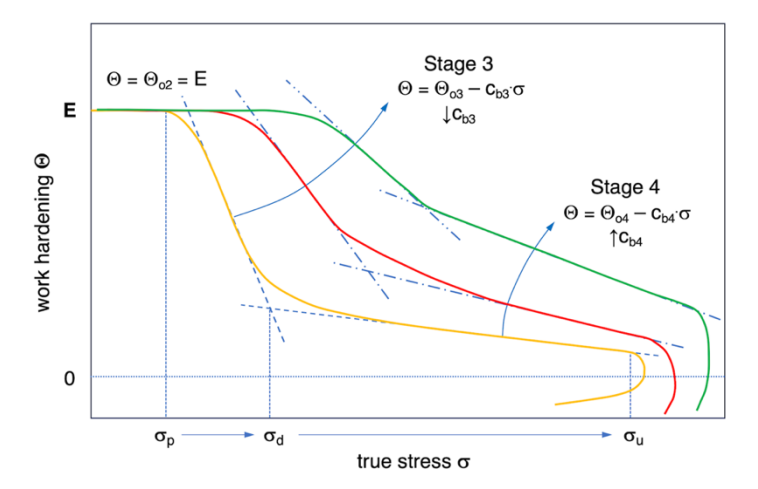


Figure 3. The work hardening $\Theta(\sigma)$ behavior is plotted beyond the elastic range as σ increases through Stage 3 and $\Theta(\sigma)$ plateaus in Stage 4 at the instability.

A relationship is explored between the softening coefficient c_{b_3} and the yield strength σ_y . It's postulated that since both c_{b3} and grain size hg will similarly vary with (and affect) strength, an analysis for the Hall-Petch behavior of $\sigma(c_{b_1})$ is proposed and quantified for Ti-6Al-4V. With the expectation that c_{b_1} will vary functionally with c_{b_2} for a constitutive relationship that spans both Stages 3 and 4, a relationship between these softening parameters can be proposed as well and expressed as $c_{b_i}(c_{b_3})$. This condition surpasses an independent behavior analysis of Stages 3 and 4, as would be approximated by sequential Voce-type behaviors. Instead, an integrated expression for work hardening is used that relates the curvilinear asymptotes produced through the sequential stages of work hardening to the instability. This $c_{\rm h}(c_{\rm h})$ relationship requires more than an approximate solution (Morris, Jr., 2007) by use of a single softening coefficient c_b; to describe a Stage 3-through-4 response, but use of a singular constitutive law that spans both stages of work hardening. Such a constitutive law is proposed (Jankowski, 2023a), wherein an asymptotic plateauing of strength occurs with increased plasticity as realized through use of a negative-exponential formulation in defining the work hardening variation $\Theta(\sigma)$ with stress. This formulation (Jankowski, 2023a) of $\Theta(\sigma)$ pursues a statistical mechanics approach to evaluate the decay in work hardening in terms of Boltzmann statistics, wherein an Arrhenius-type formulation is proposed using stress as the energetic driver.

2.2 Procedure for Analysis

The bounding conditions for the work-hardening relationship (Jankowski, 2023a) of eqn. (3) can be modeled using Stages 3-4 to provide a unique solution for determining the c_{ii} coefficients through eqns. (3a-c).

$$\Theta(\sigma) = c_{1j} \cdot e^{-(c_{2j} \cdot \sigma)}$$
(3)

$$\mathbf{c}_{\mathsf{b}_3} = -[\partial \Theta(\sigma)/\partial \sigma] \mid_{\sigma_3} = \mathbf{c}_{1\mathsf{j}} \cdot \mathbf{c}_{2\mathsf{j}} \cdot \mathbf{e}^{-(\mathsf{c}_{2\mathsf{j}} \cdot \sigma_3)} \tag{3a}$$

$$c_{b_{4}} = -[\partial\Theta(\sigma)/\partial\sigma] \Big|_{\sigma_{4}} = c_{1j} \cdot c_{2j} \cdot e^{-(c_{2j} \cdot \sigma_{4})}$$

$$c_{b_{4}} = c_{b_{3}} \cdot e^{-(c_{2j} \cdot \Delta\sigma_{3})}$$
(3b)
$$c_{b_{4}} = c_{b_{3}} \cdot e^{-(c_{2j} \cdot \Delta\sigma_{3})}$$
(3c)

$$c_{b_4} = c_{b_3} \cdot e^{-(c_{2j} \cdot \Delta \sigma_3)} \tag{3c}$$

In application, this objective is accomplished by simultaneous solution of eqns. (3a-3b) at stresses s₃ and s₄, that are representative of the slopes c_{b_3} and c_{b_4} in Stages 3 and 4, respectively. The formulation in eqn. (3c) is determined by dividing eqn. (3b) by (3a) where $\Delta \sigma$ equals the difference between the σ_4 and σ_3 stress values. The eqn. (3c) result shows that c_{b_4} will proportionally vary with c_{b_3} as a negative exponential of stress. The coefficients c_{1i} and c_{2i} (for each sample) in the work hardening relationship $\Theta(\sigma)$ of eqn. (3) provide a solution (Jankowski, 2023a) for the corresponding integral derivation of a stress-strain relationship $\sigma(\varepsilon)$ in eqn. (4), that governs plastic deformation from the onset of permanent deformation at $(\varepsilon_p, \sigma_p)$ through to the strength instability at $(\varepsilon_u, \sigma_u)$.

$$\sigma_{i}(\varepsilon) = (c_{2i})^{-1} \cdot \ln[c_{2i} \cdot (c_{1i} \cdot \varepsilon + c_{0i})] \tag{4}$$

The coefficient c_{0j} in eqn. (4) is determined (Jankowski, 2023a) by the solution of eqn. (5). In eqns. (3-4), the integral derivation allows the variable σ to be replaced by $\sigma + \sigma_0$ where σ_0 is a constant.

$$c_{oi}(\Theta, \varepsilon) = c_{1i} \cdot [(c_{2i} \cdot \Theta)^{-1} - \varepsilon]$$
(5)

The eqn. (3) coefficients can be determined by a best-fit (Jankowski, 2023a; Jankowski, 2023d) of experimental data for work-hardening $\Theta(\sigma)$ and stress-strain $\sigma(\varepsilon)$ measurements. In addition, the experimental measurement only of slopes representative of Stage 3 and 4, respectively, can be used to determine the constitutive relationships for eqn. (3) work hardening and eqn. (4) stress-strain behaviors.

3. Results

3.1 The Softening Coefficients

Additively manufactured Ti-6Al-4V samples (Leicht & Wennberg, 2015; Tao et al., 2018; Fadida et al., 2018; He et al., 2018; Voison et al., 2018) provide a data set for analysis that contains a process-dependent variation in ductility and strength. The AM methods under consideration includes electron beam melting (EBM), direct metal laser sintering (DMLS), selective laser melting (SLM), and a post-processing treatment of hot-isostatic pressing (HIP). The orientations within build plane are x and y, whereas z is the growth direction. Results of the data analysis (Jankowski, 2023a) for Ti-6Al-4V wire (Jankowski et al., 2019) and AM samples are listed in Table 1. This independently acquired data provides a basis for exploring the role of the softening coefficient c_b, in its variational relationships with the measured strength σ and the interdependency with c_{b_d} .

sample no.	1 ^(a)	2 ^(b)	3 ^(c)	4 ^(b)	5 ^(d)	6 ^(e)	7 ^(c)	8 ^(f)
material	wire	z-EBM	x-SLM+HIP	x-SLM	z-DMLS	x-SLM	z-SLM	x-SLM
c_{b_3}	1505±9	975±2	759±8	450±3	450±3	438±4	362±1	313±2
c_{b_4}	16.6±2.9	28.1±9.3	38.0±15.2	74.5±3.4	89.4±19.6	87.5±6.4	96.0±3.4	93.9±15.9
E (GPa)	118	121	120	107	122	115	107	109
Θ_{o3} (GPa)	1043±6	905±2	665±7	487±3	445±2	506±5	432±2	391±2
Θ_{o4} (GPa)	18±3	33±11	41±16	101±5	110±24	119±9	132±5	122±21
$c_{v^*} (10^{-6} \text{ nm}^3)$	4.38	5.16	7.43	10.7	12.5	10.3	12.5	14.4
$\sigma_{p}\left(MPa\right)$	640	818	762	918	788	970	940	942
$\sigma_{d}\left(MPa\right)$	689	921	865	1026	928	1102	1129	1227
$\sigma_u (MPa)$	1022	1098	1015	1283	1162	1319	1389	1284
$\epsilon_{ m pro}$	0.0054	0.0067	0.0062	0.0087	0.0065	0.0089	0.0088	0.0101
$\epsilon_{ m ult}$	0.1179	0.0830	0.0715	0.0559	0.0529	0.0458	0.0439	0.0387

Notes. (a) Jankowski et al., 2019 (b) Leicht & Wennberg, 2015 (c) Tao et al., 2018 (d) Fadida et al., 2018 (e) He et al., 2018 (f) Voison et al., 2018.

The c_{b_3} and c_{b_4} values are measurements for the slopes of Stages 3 and 4, respectively, as determined by the linear curve approximation of $\Theta(\sigma)$ that is consistent with a Voce-type stress-strain behavior. The measured elastic modulus is E. The intercepts for the work-hardening axis from Stages 3 and 4, are Θ_{o_3} and Θ_{o_4} , respectively. The coefficient c_{v^*} is defined by eqn. (2) from an evaluation (Jankowski, 2023a) of activation volume v^* . The (strain, strength) values at the proportional limit and instability are $(\epsilon_{pro}, \sigma_p)$ and $(\epsilon_{ult}, \sigma_u)$, respectively. The value of strength σ_d is determined at the extrapolated intercept between the linear approximations of Stages 3 and 4. From eqns. (3a-3c), c_{b_3} and c_{b_4} are now used to determine c_{1j} and c_{2j} for eqns. (3) and (4). A Hall-Petch relationship between c_{b_3} and the proportional limit σ_p data is plotted in Figure 4 from the experimental data listed in Table 1.

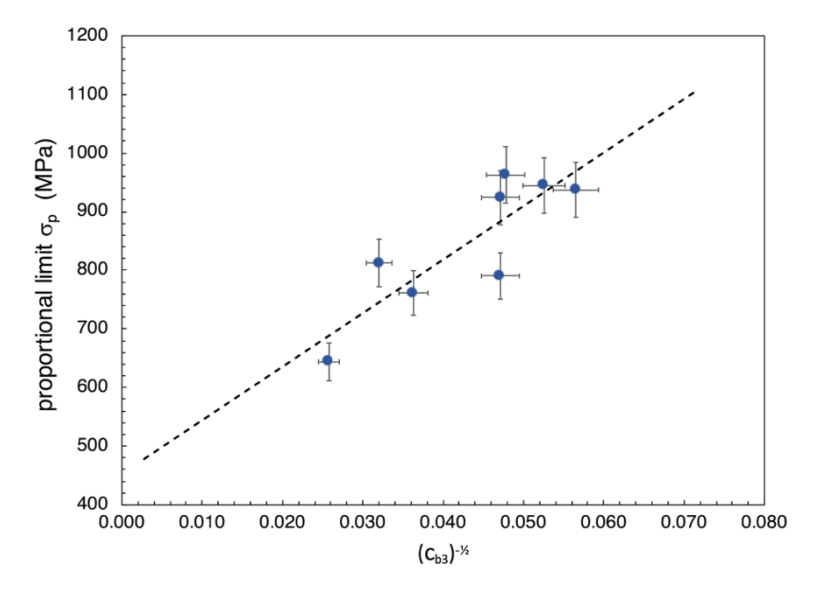


Figure 4. The strength of the Ti-6Al-4V alloy samples from different processing conditions are plotted in a Hall-Petch strengthening relationship with the slope c_{b_3} of the work hardening $\Theta(\sigma)$ curve in Stage 3, beyond the proportional limit σ_p .

From the curvilinear fit of Figure 4, the Hall-Petch relationship of eqn. (6) holds valid to a correlation coefficient R^2 of 0.74, where k_{σ} equals 9132.8 MPa and σ_{op} equals 453.0 MPa.

$$\sigma_{p} = k_{\sigma} \cdot (c_{b_{3}})^{-1/2} + \sigma_{op} \tag{6}$$

The functional relationship between c_{b_4} and c_{b_3} as derivative from eqn. (3) can be assessed using eqn. (3c) for *each* individual sample, using the corresponding unique values for c_{b_3} , c_{2i} , and $\Delta \sigma$.

A general relationship to assess c_{b_4} as a functional variation of c_{b_3} is presented in the negative-exponential formulation of eqn. (7) as a direct derivative from eqn. (3).

$$c_{b_4} = c_{3j} \cdot e^{-(c_{4j} \cdot c_{b_3})} \tag{7}$$

Eqn. (7) provides a means for assessing the $c_{b_4}(c_{b_3})$ relationship between independent experimental measurements of c_{b_4} and c_{b_3} for all samples. This approach is pursued since the variable $\Delta \sigma$ in the exponent of eqn. (3c) is found to be a function of c_{b_3} , as verified in the validity of eqn. (6) to fit the Hall-Petch plot of Figure 4. The values to be determined for the dimensionless coefficients c_{3j} and c_{4j} are representative of the Ti-6Al-4V alloy system, in comparison to the c_{0j} , c_{1j} and c_{2j} values of eqns. (3-5) that are determined individually for each sample within the alloy system. The $c_{b_4}(c_{b_3})$ variation is plotted in Figure 5 using the data listed in Table 1.

The negative-exponential curvilinear fit of the Figure 5 data using eqn. (7) holds valid to a correlation coefficient R^2 of 0.95, where the dimensionless coefficient(s) c_{3j} equals 160.2 and c_{4j} equals 0.00161. Analogous to the representation in eqn. (6), a Hall-Petch construct using c_{b_4} can be made by substituting eqn. (7) into (6) wherein the strength σ would vary as a linear function of inverse square-root, i.e. ($\ln c_{b_4}$)- $^{1/2}$.

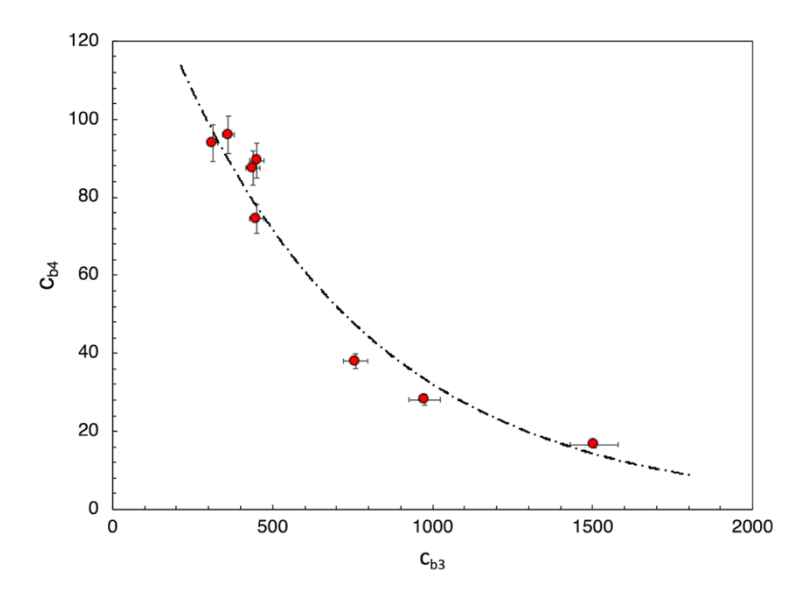


Figure 5. The continuous curve produced by the negative-exponential of work hardening $\Theta(\sigma)$ infers a negative-exponential formulation of the coefficients c_{b_3} and c_{b_4} as plotted using eqn. (7)

3.2 Simulations of Work Hardening

A simulation of the stress-strain behavior using eqn. (4) is integral with the analysis of the work hardening formulation of eqn. (3), as documented (Jankowski, 2023a) using a fit of all experimental data derivative to the original stress-strain measurements. The Sec. 4.1 results found using just the one work hardening formulation of eqn. (3) now provides a means to predict Stage 4 behavior from that of Stage 3, as seen in the Figure 5 results using eqn. (7). Therefore, a unique solution to eqn. (4) to simulate the entire stress-strain response requires use of only two data points (i.e. one each from Stage 3 and 4) along with measured values of c_{b_3} and c_{b_4} , in comparison to a fit of the entire work-hardening data set. A *two point-slope fit* method using eqns. (3a-3c) determines the values for the c_{1j} and c_{2j} used in eqns. (3), (4), and (5). The results using three different *two point-slope fit* data sets are listed in Table 2.

Table 2. Results of two-point-slope fit analysis for AM Ti-6Al-4V

sample no.			1 ^(a)	2 ^(b)	3 ^(c)	4 ^(b)	5 ^(d)	6 ^(e)	7 ^(c)	8 ^(f)
c_{ij}	σ_3	σ_4	wire	z-EBM	x-SLM+HIP	x-SLM	z-DMLS	x-SLM	z-SLM	x-SLM
	all data		9.121	$2.191 \cdot 10^5$	$2.124 \cdot 10^6$	636.2	93.04	1696	195.4	$3.675 \cdot 10^4$
c_{1j}	$\sigma_{_p}$	$\sigma_{\rm u}$	238.3	2428	531.2	8.390	3.136	8.328	1.971	2.453
$(10^6 \mathrm{MPa})$	$\sigma_{_{pd}}$	$\sigma_{\rm u}$	1235	$4.936 \cdot 10^6$	$1.214 \cdot 10^6$	83.80	39.58	209.0	22.58	$2.914 \cdot 10^9$
	$\sigma_{ m pd}$	σ_{du}	$2.014 \cdot 10^7$	$1.329 \cdot 10^9$	$4.395 \cdot 10^7$	2326	237.7	1828	59.84	112.9
	all data		8.973	17.85	21.61	9.688	8.632	10.05	7.744	12.71
c_{2j}	$\sigma_{_{p}}$	$\sigma_{\!_{u}}$	11.77	12.66	11.84	4.923	4.321	4.612	2.956	3.522
(10 ⁻³ MPa ⁻¹)	$\sigma_{\rm d}$	$\sigma_{\rm u}$	13.52	20.02	19.98	6.990	6.907	7.415	5.105	21.20
	$\sigma_{_{pd}}$	$\boldsymbol{\sigma}_{\!\scriptscriptstyle du}$	23.55	25.32	23.68	9.846	8.642	9.224	5.912	7.045
	all data		0.02279	1288	$1.244 \cdot 10^4$	4.764	0.5042	13.33	1.434	356.9
-c _{oj}	$\sigma_{_{p}}$	$\sigma_{\!_{u}}$	1.131	13.81	2.575	0.0541	0.0135	0.0548	0.0118	0.01682
(MPa)	σ_{d}	$\sigma_{\rm u}$	6.262	$3.249 \cdot 10^4$	727.8	0.6390	0.2254	1.673	0.1739	$2.927 \cdot 10^7$
	$\boldsymbol{\sigma}_{pd}$	$\boldsymbol{\sigma}_{du}$	$1.088 \cdot 10^5$	$8.881 \cdot 10^6$	$2.681 \cdot 10^{5}$	19.31	1.450	15.36	0.4800	1.026

Notes. (a) Jankowski et al., 2019 (b) Leicht & Wennberg, 2015 (c) Tao et al., 2018 (d) Fadida et al., 2018 (e) He et al., 2018 (f) Voison et al., 2018.

The two points used to uniquely determine all coefficients of eqns. (3) and (4) are listed in Table 2 as σ_3 and σ_4 corresponding to Stages 3 and 4, respectively. In addition to previously defined σ_p , σ_d and σ_u , the midpoints of Stages 3 and 4 are σ_{pd} and σ_{du} , respectively. These four strength values are the input values for σ_3 and σ_4 , as used in eqns. (3a-3c), to compute the coefficients of eqns. (3) and (4). A comparison of the corresponding simulated $\Theta(\sigma)$ and $\sigma(\varepsilon)$ curves produced from eqns. (3) and (4) are shown in Figs. 6 and 7, respectively. The three cases considered in Figs. 5-6 for input σ_3 and σ_4 values are: (σ_p to σ_u) the strengths at the proportional limit σ_p and instability σ_u ; (σ_d to σ_u) the strengths at the Stage 3-4 intercept σ_d and the instability σ_u ; and (σ_{pd} to σ_{du}) the midpoint strength values within Stages 3 and 4, respectively. For each case, the measured c_{b_3} and c_{b_4} values are used as listed in Table 1. In these two figures, samples no. 1, 3, 5, and 7 are selected as representative of the variation in yield-strength data set of the Table 1. The previous (Jankowski, 2023a) full fit curve of 'all data' for the work hardening curves in Figure 6 to determine c_{1j} and c_{2j} closely overlay the experimental data. The use of a two point-slope fit solution (now selecting a stress σ_3 and σ_4 in each Stage 3 and 4, respectively) readily provides an assessment approach that can prove useful for modeling (noisy) work hardening data with a constitutive relationship.

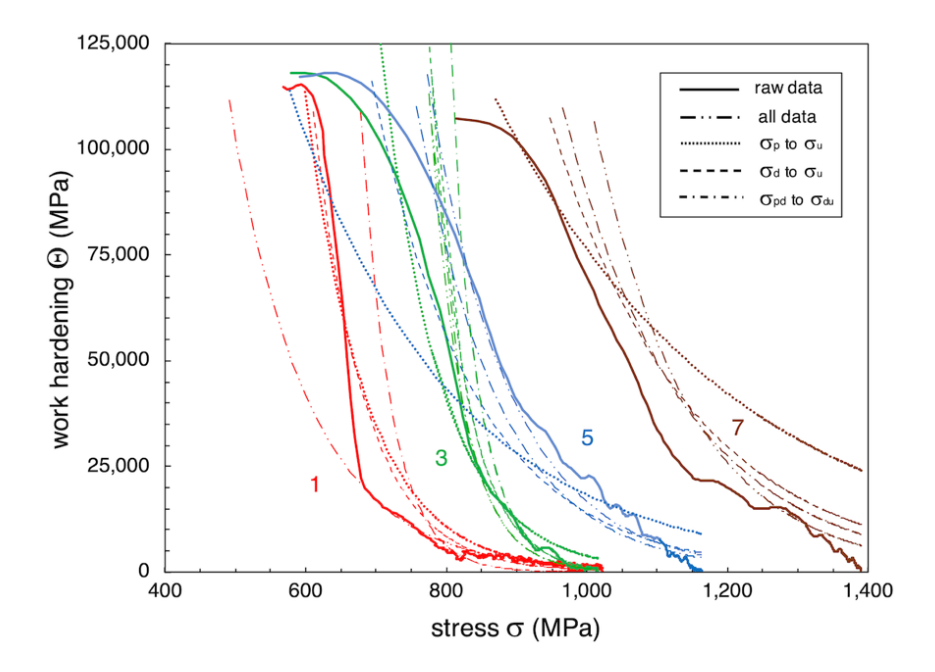


Figure 6. The $\Theta(\sigma)$ plots for samples no. 1, 3, 5, and 7 are representative of the raw data (solid line) and eqn. (3) simulations that use all data (dash-double dot line) and stress values at two points within Stages 3 and 4: σ_p to σ_u (dotted curve); σ_d to σ_u (dashed curve); and σ_{pd} to σ_{du} (dot-dashed curve).

4. Discussion

The development of the modeling efforts is motivated by a need to provide a basis for comparing and evaluating the wide range of mechanical behaviors observed in crystalline structural alloys as processed under rapid solidification, and as often subjected to aging treatments to normalize these effects. Advantage can be taken of the wide range of behaviors in the selective choice of materials strengths that can made in topology optimized designs through additive manufacturing. For example, in the specification of high strength at a stress point, and the specification of ductility at a location of desired plasticity. This method provides a means to determine and specify parameters using the softening coefficients, and the interrelationship provided in the constitute nonlinear work-hardening formulation - to design, test and approve materials performance in applications such as automotive and aerospace components. The use of the data selected from the literature need be suitable for this intended purpose, and as such, has proven challenging. Often, conventional tensile loading under constant strain-rate conditions produces oscillations in the stress level, leading to unusable data for work hardening analysis due to high-frequency stress-strain slope inversions.

The asymptote fit of curvilinear $\Theta(\sigma)$ behavior to Stages 3 and 4 determines c_{b_3} and c_{b_4} values that are consistent with the present attempt to model the entire plastic range of deformation, from the proportional limit to the strength instability, using a single expression which includes both features of rapid work hardening and a leveling of strength as shown in Figure 1. This specific negative-exponential eqn. (3) formulation of work hardening $\Theta(\sigma)$ is directly integral to the corresponding eqn. (4) stress-strain relationship.

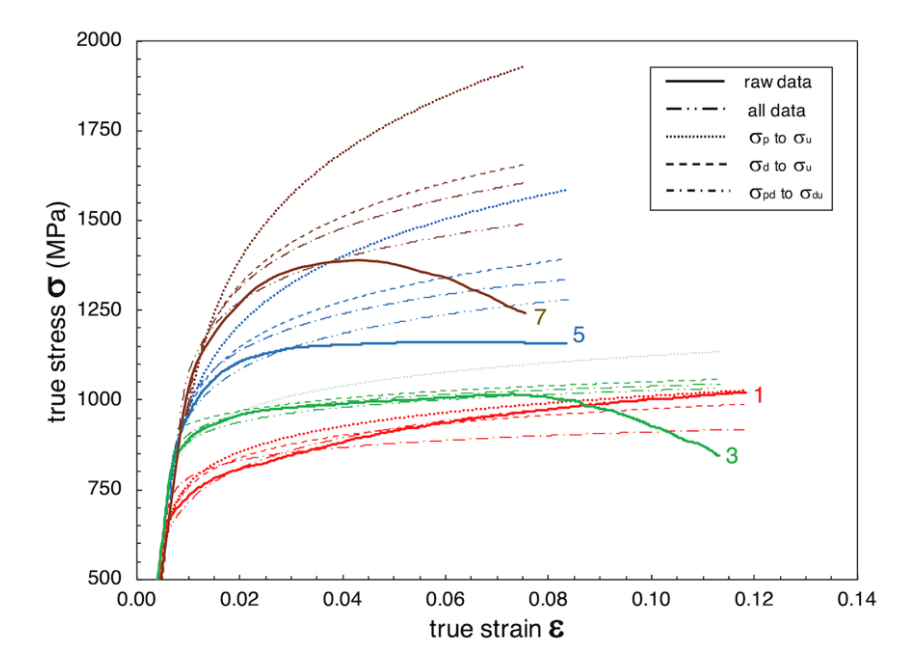


Figure 7. The true stress-strain curves for samples no. 1, 3, 5, and 7 are representative of the raw data (solid line) and eqn. (4) simulations using the c_{oj} , c_{1j} and c_{2j} values determined from the $\Theta(\sigma)$ analysis of Figure 6 for all data (dash-double dot line) and stress values at two points within Stages 3 and 4: σ_p to σ_u (dotted curve); σ_d to σ_u (dashed curve); and σ_{pd} to σ_{du} (dot-dashed curve).

As for samples no. 1, 3, 5, and 7 in Figure 6, the Voce simulation doesn't replicate (Jankowski, 2023a) the Stage 3 response for the stress-strain $\sigma(\epsilon)$ curves of any sample listed in Table 1 but can work well for Stage 4. On general, although the Hollomon expression doesn't replicate Stage 4, it well simulates the rapid rise in work hardening of Stage 3 stress-strain behavior. At present, only the stress-strain relationship of eqn. (4) simulates the range of results shown in Figure 7, as generated from the work hardening relationship of eqn. (3). The $\Theta(\sigma)$ results of Figure 6 span the range from a rapid decrease of work hardening (that begins at the proportional limit) and progresses to its leveling (as stress increases to the instability). For the *two point-slope fit* method, the combination of the σ_{pd} to σ_{du} pair of input data points (at midspan to each of Stage 3 and 4) appears to best simulate the experimental curves plotted in both Figures 6 and 7.

The decrease in c_{b_4} seen in Figure 5 occurs with an increase in c_{b_3} , as found in Figure 5. The total plastic strain increases as c_{b_4} decreases (and c_{b_3} increases). From eqn. (1), assuming a slowly varying (or near constant) activation volume v^* , the m-value would trend to increase with increasing c_{b_3} as computed from the Table 1 data. The approach to determine the c_{l_j} and c_{2_j} values (from the c_{b_3} and c_{b_4} values) assumes the slope midway to Stages 3 and 4 as best representative to establish a functional $\Theta(\sigma)$ relationship. This may not always be the case as is found (Jankowski & Yee, 2023a) for steels subject to martensitic transformations wherein the $\Theta(\sigma)$ response can be affected by the onset of phase transformations during deformation and through thermal transients.

Material properties are well known to vary with grain size. Observations of general trends can be made in the variation of strength and strain rate sensitivity as shown in Figure 2. Formulations have been widely developed that relate the strain-rate sensitivity of strength exponent m with the activation volume v^* of defect mobilization at the onset of plastic deformation. Recently, the activation volume is formulated (Jankowski, 2023a) in eqns. (1-2) as a function of the softening coefficient c_{b_3} from the Stage 3 region of work hardening, i.e., the slope of the Figure 3 work hardening curve $\Theta(\sigma)$ following the proportional limit. Although the softening coefficient is dimensionless, these observations (in combination) provide the basis to postulate that c_b is representative of microstructural scale, as can be inferred from previous (Morris, Jr., 2007) investigation. The 1st postulate of using the Stage 3 softening coefficient as a surrogate for grain size is successfully assessed using a Hall-Petch formulation of $\sigma(c_{b_3})$ as plotted in Figure 4.

The region of extended plastic deformation beyond rapid work hardening is often manifest as a steady state behavior. The approximation of using a linear fit for the work hardening $\Theta(\sigma)$ is represented by the softening

coefficient c_{b_4} for Stage 4. These two stages are postulated (Jankowski, 2023a) as representative of different attributes of a single constitutive relationship for work hardening behavior as shown in eqn. (3), where an Arrhenius behavior is proposed for the evolution of work hardening with increasing stress. As the softening coefficients can be represented as tangents to this eqn. (3) at the early and late stages of deformation, an expression is derived in eqn. (7) that represents the interdependency of these coefficients. A negative exponential function of eqn. (7) is successfully plotted in Figure 5 using independent experimental measurements of Stage 3 and 4 c_{bi} behavior. The 2^{nd} postulate is validated that work hardening can be modeled using a single constitutive behavior in contrast to be requiring *separate* behaviors for rapid and slow (steady-state) work hardening.

A novel approach is used to generate simulations of the work hardening $\Theta(\sigma)$ and stress-strain behavior $\sigma(\epsilon)$ using the formulations presented in eqns. (3) and (4). In the 3rd postulate, for deploying a *two point-slope fit* approach, only a data point from each of Stages 3 and 4 is needed to uniquely solve simultaneous equations for determining all the coefficients for the $\Theta(\sigma)$ and $\sigma(\epsilon)$ relationships. In addition to a best fit using all data points, the simulation works well using just a midpoint within each of Stages 3 and 4 to replicate the experimental behavior.

5. Summary

The sequential stages of work hardening beyond the proportional limit up to the instability are considered in a unified work hardening relationship. The connection between the Stage 3 and 4 work hardening allows for predictive behavior from one work hardening stage to the other. Along with a successful reproduction of the stress-strain response, the tenets of rapid work hardening followed by a steady state response are unified through a single constitutive response wherein the determination of all softening coefficients can be expedited by a two point-slope fit.

The advent of topology optimized designs can extend beyond the necessity for use of material stock with uniform properties as is often deployed for conventional machining or sought through post casting heat treatments. For additively manufactured components, there is an advantage to specifying and controlling the mechanical properties selectively throughout the build. The use of softening coefficients c_{b_3} and c_{b_4} provides a convenient means to envelope strength and ductility in a useable and quantifiable fashion for this purpose in design, qualification, testing, and acceptance criteria. A codification of the scripts that have been recently developed (in part) to apply the method for the determination and specification of softening coefficients will be made available for use, with an initial application for examining the aging behavior of AM stainless steel.

Acknowledgments

The effort for this work was inspired by the objective to enhance the engineering application of structural AM materials. Any subjective views or opinions that might be expressed in the paper do not necessarily represent the views of the US Department of Energy or the United States Government. Sandia National Laboratories is a multimission laboratory managed and operated by National Technology & Engineering Solutions of Sandia, LLC, a wholly owned subsidiary of Honeywell International Inc, for the US Department of Energy's National Nuclear Security Administration under contract DE-NA0003525. Data from which the modeling and simulations in this paper are made is available in the literature referenced and upon request.

References

- Considère, A. (1885). Mémoire sur lemploi du fer et de lacier dans les constructions. *Anales des Ponts et Chaussées*, 9, 574-775.
- Dao, M., Lu, L., Asaro, R. J., De Hosson, J. T. M., & Ma, E. (2007), Toward a quantitative understanding of mechanical behavior of nanocrystalline metals. *Acta Materialia*, *55*, 4041-4065. https://doi.org/10.1016/j.actamat.2007.01.038.
- Fadida, R., Shirizly, A., & Rittel, D. (2018). Dynamic tensile response of additively manufactured Ti-6Al-4V with embedded spherical pores. *Journal of Applied Mechanics*, 85, 41004-1-10. https://doi.org/10.1115/1.4039048.
- Gu, C. D., Lian, J. S., Jiang, Q., & Zheng, W. T. (2007). Experimental and modeling investigations on strain rate sensitivity of an electrodeposited 20 nm grain sized Ni. *Journal of Physics D: Applied Physics*, 40, 7440-7446. https://doi.org/10.1088/0022-3727/40/23/027.
- He, B., Wu, W., Zhang, L., Lu, L., Yang, Q., Long, Q., & Chang, K. (2018). Microstructural characteristic and mechanical property of Ti-6Al-4V alloy fabricated by selective laser melting. *Vacuum*, *150*, 79-83. https://doi.org/10.1016/j.vacuum.2018.01.026
- Hollomon, J. H. (1945). Tensile Deformation. Trans AIME, 162, 268-290.

- Humphrey, R. T., & Jankowski, A. F. (2011). Strain-Rate Sensitivity of Strength in Macro-to-Micro-to-Nano Crystalline Nickel, *Surface and Coatings Technology*, *206*, 1846-1849. https://doi.org/10.1016/j.surfcoat.2011.08.010.
- Jankowski, A. F., & Nyakiti, L. O. (2010), Anomalies in Hall-Petch Strengthening for Nanocrystalline Au-Cu Alloys Below 10 nm Grain Size. *Surface and Coatings Technology*, 205, 1398-1402. https://doi.org/10.1016/j.surfcoat.2010.07.106.
- Jankowski, A. F., Chames, J. M., Gardea, A., Nishimoto, R., & Brannigan, E. M. (2019). The softening factor c_b of commercial titanium alloy wires. (*Zeitschrift fuer Metallkunde*) *International Journal of Materials Research*, 110, 990-999. https://doi.org/10.3139/146.111834.
- Jankowski, A. F., Yang, N., & Lu, W-Y. (2020). Constitutive structural parameter c_b for the work hardening behavior of laser powder-bed fusion, additively manufactured 316L stainless steel. *Material Design and Processing Communication* 2020, e96-1-9. https://doi.org/10.1002/mdp2.135.
- Jankowski, A. F. (2021). A constitutive structural parameter c_b for the work hardening behavior of additively manufactured Ti-6Al-4V. *Material Design and Processing Communication*, 2021, e262-1-9. https://doi.org/10.1002/mdp2.262.
- Jankowski, A. F. (2023a). On the origin of stress-strain relationships, the evaluation if softening coefficients and mechanistic models for work hardening. *Materials Science and Engineering A*, 882, 145472-1-14. https://doi.org/10.1016/j.msea.2023.145472
- Jankowski, A. F. (2023b). On the constitutive stress-strain relationships and evaluation of the softening coefficient in work hardening mechanism. *Sandia National Laboratory*, SAND2023-00634.
- Jankowski, A. F. (2023c). A model for the softening factor within stages of work hardening. *Sandia National Laboratory*, SAND2023-00635.
- Jankowski, A. F. (2023d). On a new constitutive stress-strain relationship in the evaluation of nonlinear work hardening behavior. *Sandia National Laboratory*, SAND2023-02795.
- Jankowski, A. F., & Yee, J. K. (2023a). Stress-strain and work hardening relationships of 304L AM alloy. *Sandia National Laboratory*, SAND2023-11259.
- Jankowski, A. F., & Yee, J. K. (2023b). An approach to determine the softening coefficients of work hardening in Al 6061. *Sandia National Laboratory*, SAND2023-14862.
- Kocks, U. F., & Mecking, H. (2003). Physics and phenomenology of strain hardening: the FCC case. *Progress in Materials Science*, 48, 171-273. https://doi.org/10.1016/S0079-6425(02)00003-8.
- Leicht, A., & Wennberg, E. (2015). Analyzing the Mechanical Behavior of Additive Manufactured Ti-6Al-4V Using Digital Image Correlation. Diploma Work No. 157. SP Technology Research Institute of Sweden, Chalmers University of Technology, Gothenburg, p. 51.
- Morris Jr., J. W. (2007). Is there a future for nanostructured steel? in 16th International Society for Offshore and Polar Engineering Conf Proc. ISOPE, 2007, 2814-2818.
- Nyakiti, L. O., & Jankowski, A. F. (2010). Characterization of strain-rate sensitivity and grain boundary structure in nanocrystalline gold-copper alloys. *Metallurgical and Materials Transactions A*, 41, 838-847. https://doi.org/10.1007/s11661-009-9996-9.
- Tao, P., Li, H-X., Huang, B-Y., Hu, Q-D., Gong, S-L., & Xu, Q-Y. (2018). Tensile behavior of Ti-6Al-4V alloy fabricated by selective laser melting: effects of microstructures and as-built surface quality, *Research Development China Foundry*, 15(4), 243-252. https://doi.org/10.1007/s41230-018-8064-8.
- Voce, E. (1948). The Relationship Between Stress and Strain for Homogeneous Deformation. *J. of the Institute Metals* 74, 537-562.
- Voisin, T., Calta, N. P., Khairallah, S. A., Forien, J-B., Balogh, L., Cunningham, R. W., Rollett, A. D., & Wang, Y. M. (2018). Defects-dictated tensile properties of selective laser melted Ti-6Al-4V. *Material Design*, *158*, 113-126. https://doi.org/10.1016/j.matdes.2018.08.004.
- Wei, Q., Cheng, S., Ramesh, K. T., & Ma, E. (2004). Effect of nanocrystalline and ultrafine grain sizes on the strain rate sensitivity and activation volume: fcc versus bcc metals. *Materials Science and Engineering A*, 381, 71-79. https://doi.org/10.1016/j.msea.2004.03.064

Copyrights

Copyright for this article is retained by the author(s), with first publication rights granted to the journal.

This is an open-access article distributed under the terms and conditions of the Creative Commons Attribution license (http://creativecommons.org/licenses/by/4.0/).